IOP Publishing Nanotechnology
Nanotechnology 32 (2021) 415703 (8pp) https://doi.org/10.1088/1361-6528/ac1095

Modification of interface and electronic transport in van der Waals heterojunctions by UV/O_3

Xiaoqing Ma[1,2], Yanqi Mu[2,3], Guancai Xie[2,3], Hongfeng Wan[2,3], Weixuan Li[2], Mengshan Li[1,2], Haitao Dai[1,*], Beidou Guo[2,3,*] and Jian Ru Gong[2,3,*]

[1] Tianjin Key Laboratory of Low Dimensional Materials Physics and Preparing Technology, School of Science, Tianjin University, Tianjin 300072, People's Republic of China
[2] Chinese Academy of Sciences (CAS) Center for Excellence in Nanoscience, CAS Key Laboratory of Nanosystem and Hierarchy Fabrication, National Center for Nanoscience and Technology, Beijing 100190, People's Republic of China
[3] University of CAS, Beijing 100190, People's Republic of China

E-mail: gongjr@nanoctr.cn, guobd@nanoctr.cn and htdai@tju.edu.cn

Received 30 March 2021, revised 9 June 2021
Accepted for publication 1 July 2021
Published 20 July 2021

Abstract

Two-dimensional (2D) van der Waals heterojunctions have many unique properties, and energy band modulation is central to applying these properties to electronic devices. Taking the 2D graphene/MoS_2 heterojunction as a model system, we demonstrate that the band structure can be finely tuned by changing the graphene structure of the 2D heterojunction via ultraviolet/ozone (UV/O_3). With increasing UV/O_3 exposure time, graphene in the heterojunction has more defect structures. The varied defect levels in graphene modulate the interfacial charge transfer, accordingly the band structure of the heterojunction. And the corresponding performance change of the graphene/MoS_2 field effect transistor indicates the shift of the Schottky barrier height after UV/O_3 treatment. The result further proves the effective band structure modulation of the graphene/MoS_2 heterojunction by UV/O_3. This work will be beneficial to both fundamental research and practical applications of 2D van der Waals heterojunction in electronic devices.

Supplementary material for this article is available online

Keywords: band structure, graphene/MoS_2, heterojunction, UV/O_3

(Some figures may appear in colour only in the online journal)

1. Introduction

Owing to the atomic thickness and high-quality layer structure, two-dimensional (2D) van der Waals heterojunctions display many new properties [1–3], such as large bandgap range from conductor to insulator [4] and resistance to short channel effects of the field effect transistor (FET), and enabling the ultimate dimensional scaling [5], which have great development prospects in future electronic device applications. These properties can be modulated by a few methods, such as element doping, defect engineering, surface modification/functionalization, and adding interlayer materials [5–9], which change the geometry and electronic structure of 2D materials. For instance, inserting h-BN at the interface of the MoS_2/graphene heterojunction can avoid the interlayer carrier coupling and restore the photovoltaic effect of the heterojunction [10]. After annealing treatment, the adsorbates/impurities at the interface of the MoS_2/graphene heterojunction can be removed, which promotes the interfacial charge transfer [11].

Ultraviolet ozone (UV/O_3) has aroused great interest as an easily-controlled method of regulating 2D materials. For example, UV/O_3 can oxidize graphene to obtain larger chemical surface-enhanced Raman scattering [8]. For device

* Authors to whom any correspondence should be addressed.

fabrication applications, UV/O_3 can be used to aid in the removal of polymethyl methacrylate (PMMA) residues in the transfer and photolithographic processing of 2D materials such as MoS_2 produced by sulfurization [12]. It also can be used to increase the surface energy of MoS_2 by form the weak sulfur–oxygen bond, allowing the subsequent deposition of the uniform Al_2O_3 thin film by atomic layer deposition [13, 14], which is helpful for the preparation of the dielectric layer of top-gate FET. UV/O_3 with appropriate treatment time can be used to improve the quality of graphene and reduce electrical resistance [15]. In addition, the effect of UV/O_3 on the oxidation of 2D materials such as MoS_2 is also affected by crystallinity, resulting in different oxidation results [16]. However, most related works focus on the role of a single material. Study on the influence of material components on 2D heterojunctions, which leads to the evolution of the band structure property and the related device performance during the UV/O_3 treatment, is needed for further development and applications of 2D heterojunctions.

In this work, we investigate the influence of UV/O_3 on the band structure of the 2D graphene/MoS_2 van der Waals heterojunction. The reason to choose this model system is because graphene is the first well-studied 2D material with ultrahigh carrier mobility and, MoS_2 is currently intensively investigated channel material because of its sizable bandgap in the range of 1.2–1.8 eV [17]. The results show that the structural changes can modulate the charge transfer between MoS_2 and graphene, resulting in changes in the band structure of the heterojunction. And the change of the electrical transport characteristics of the graphene/MoS_2 FET is due to the shift of the Schottky barrier height, that is, the change of the band structure of the heterojunction after UV/O_3 treatment. This work provides an in-depth understanding on modulation of the interface charge transfer by UV/O_3 tuning the component structure in the 2D heterojunctions.

2. Experimental section

2.1. Graphene/MoS_2 heterojunction preparation

The monolayer MoS_2 is prepared by chemical vapor deposition (CVD). Sulfur powder (99.5%, J&K Scientific) and MoO_3 (molybdenum oxide, 98%, Ourchem) are used as growth precursors, and NaCl (99.7%, Sinopharm) is used as a catalyst to grow MoS_2 under atmospheric pressure. High-purity argon is used as the protective gas for the growth process, and its flow rate is 50 sccm. The SiO_2/Si substrate is placed facing down on the top of the MoO_3 source. The MoO_3 is heated first, the temperature is increased to 500 °C after 25 min, and then to 750 °C after 25 min and maintains for 10 min. When MoO_3 is 380 °C, the sulfur powder is increased to 120 °C after 10 min. After the reaction is over, the furnace is turned on and cooled to room temperature. The monolayer CVD graphene is purchased from Shanghai Onway Technology Co., Ltd.

The monolayer graphene and MoS_2 are prepared by CVD. The PMMA photoresist layer employed to provide mechanical support is spin-coated on the $MoS_2/SiO_2/Si$ and graphene/Cu, and cured at 180 °C for 2 min. Then the SiO_2/Si and Cu substrates are etched, and the PMMA/MoS_2 and PMMA/graphene films are washed multiple times with ultrapure water in order to remove residues. The PMMA/MoS_2 film is transferred onto the N^+ doped Si substrate covered with 300 nm thick SiO_2, and then dried in a vacuum oven at 80 °C for 30 min. The PMMA layer in PMMA/$MoS_2/SiO_2/Si$ is removed in acetone to get the as-transferred MoS_2 sample. The same method is used to transfer PMMA/graphene film to the as-transferred MoS_2 and SiO_2/Si substrate to obtain the graphene/MoS_2 heterojunction and graphene control samples.

The monolayer MoS_2 and monolayer graphene are mechanically exfoliated from bulk crystals purchased from Shanghai Onway Technology Co., Ltd. First, we tear the bulk graphene and MoS_2 with tape, and then past them on the polydimethylsiloxane (PDMS) film, respectively. After finding monolayer graphene and monolayer MoS_2 on PDMS film through optical microscopy, the MoS_2/PDMS film is aligned and contacted with the SiO_2/Si substrate through the transfer platform. After heating at 60 °C for two minutes, carefully lift the PDMS film. Finally, monolayer MoS_2 remains on the substrate. Similarly, the monolayer graphene is appropriately overlapped with the as-transferred MoS_2 through the transfer platform to obtain the graphene/MoS_2 heterojunction.

2.2. Graphene/MoS_2 FET fabrication

The mechanically exfoliated monolayer MoS_2 and monolayer graphene are transferred to the N^+ doped Si substrate covered with 300 nm thick SiO_2 sequentially, assembling a graphene/MoS_2 heterojunction. Subsequently, the metal electrodes are deposited using electron beam lithography and thermal evaporation of Cr/Au (5 nm/50 nm). For UV/O_3 treatment, a window is only opened on the graphene between source and drain electrodes by electron beam lithography.

After PMMA photoresist is spin-coated on the surface of graphene/MoS_2 heterojunction, electron beam exposure is performed to open a window on the top of graphene, as shown in the orange solid box in figure 7(b). Since other area is protect by PMMA, only the graphene at the exposure window area can generate defects under UV/O_3 treatment.

2.3. Characterization

The UV/O_3 treatment is conducted in UV ozone cleaner (Ossila). Optical images are taken by Olympus BX53M microscope. Both Raman spectra and PL measurements are characterized by Raman spectroscopy (Renishaw inVia plus) equipped with a 514 nm laser. The XPS spectra are characterized by Ulvac-PHI Quantera II. The electrical characteristics are measured by a PDA FS-Pro semiconductor parameter analyzer with a probe station.

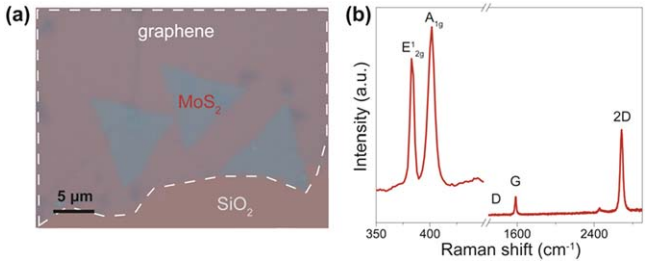

Figure 1. (a) Optical image of the graphene/MoS_2 heterojunction on the SiO_2/Si substrate. (b) The Raman spectrum of graphene and MoS_2.

3. Result and discussion

First, we prepare graphene/MoS_2 heterojunction samples and graphene control samples used in the experiment. Graphene and MoS_2 are prepared by CVD with high-quality and large area. As shown in figure 1(a), MoS_2 is in the shape of a flake triangle, and covered by a large area of graphene (white dashed box).

In order to obtain the structural information of the as-prepared graphene and MoS_2 materials, Raman spectroscopy [18, 19], which is non-destructive, fast and high sensitivity [20, 21], is carried out. As shown in figure 1(b), the Raman spectrum of graphene displays the G peak near 1580 cm^{-1}, which is related to the vibration of carbon hexagonal rings of graphene, and the 2D peak with a signature at about 2700 cm^{-1}. The intensity ratio of the 2D peak to the G peak (I_{2D}/I_G) is >2, proving that graphene is a monolayer. The D peak with a signature for the disorder at about 1345 cm^{-1} is not observable, indicating the high-quality of graphene with little defects [22]. The Raman spectrum of MoS_2 in figure 1(b) exhibits two obvious characteristic peaks at 383 and 401 cm^{-1}, which designates the in-plane Mo–S phonon mode (E^1_{2g}) and the out-of-plane Mo–S mode (A_{1g}). The distance between the E^1_{2g} peak and the A_{1g} peak is 18 cm^{-1}, corresponding to the monolayer MoS_2 [23, 24]. The above data validate that both graphene and MoS_2 used in our experiment are monolayer.

Next, we examine the effect of UV/O_3 exposure on the structure of the graphene/MoS_2 heterojunction and graphene by Raman spectroscopy. As the UV/O_3 treatment time increases from 0 to 5 min, the D peak intensity of the graphene/MoS_2 heterojunction roughly gradually increases, indicating the defects in the graphene increase in figure 2(a). Especially, the D peak dramatically enhances at the 5 min together with the appearance of the D′ peak at about 1610 cm^{-1}, displaying a further increase of defects. As shown in figure 2(b), we calculate the peak intensity ratio of I_G/I_D which can accurately reflect the defects change according to figure 2(a). The increasing ratio of I_G/I_D represents the size of in-plane crystallites formed by a certain number of carbon rings is getting smaller, that is, graphene has more defects. However, the increase in I_G/I_D of heterojunction from 0 to 1 min is negligible, indicating that there is almost no change in defects. Moreover, as the exposure time exceeds 1 min, the I_G/I_D of heterojunction increase notably, indicating that the

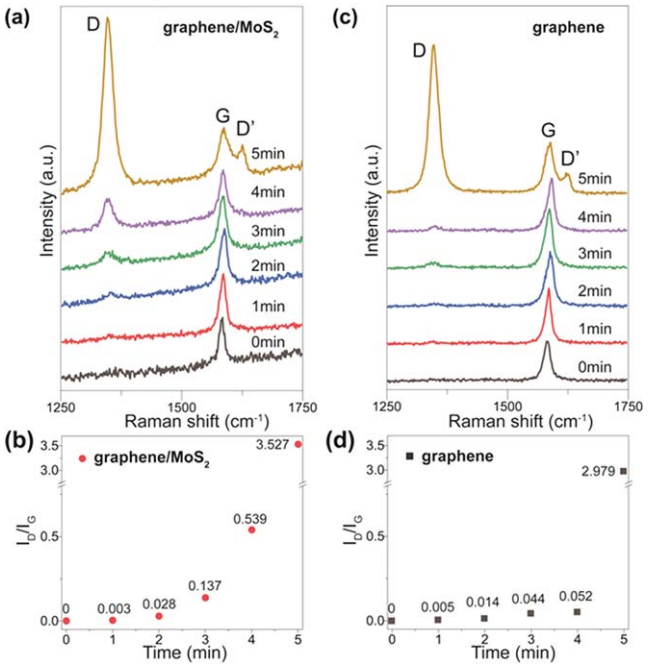

Figure 2. Raman spectra and the intensity ratio of I_D/I_G of the graphene/MoS_2 heterojunction (a), (b) and graphene (c), (d) with the UV/O_3 treatment from 0 to 5 min, respectively.

defects are gradually increasing. The graphene control sample has a similar changing trend for both D peak and I_G/I_D in figures 2(c) and (d) compared to graphene/MoS_2 heterojunction. Compared the 0 min treatment time, it can be seen in figure 2 that the G peak has a very obvious broadening when the treatment time is 5 min, indicating the increase of defects [25, 26]. The difference between the two samples is that graphene/MoS_2 has more defects than graphene for the UV/O_3 treatment from 1 to 5 min. We have also added the error bar in the I_D/I_G of Raman spectra of heterojunction and graphene Raman spectroscopy, and the results are similar (see figure S1 available online at stacks.iop.org/NANO/32/415703/mmedia, supporting information). This is proved that graphene can generate more defects by UV/O_3 due to its contact with MoS_2 to form a heterojunction.

To characterize the structures of the graphene/MoS_2 heterojunction and graphene after UV/O_3, micro x-ray photoelectron spectroscopy (XPS) is used to investigate the different chemical structures of the graphene/MoS_2 heterojunction and graphene with an exposure time of 4 min. The energy resolution is less than 0.48 eV, and the minimum value of the focused x-ray beam is 7.5 μm, coupled with the aid of a microscope, so the target test points can be accurately located. As shown in figure 3(a), the XPS spectrum of C1s for graphene/MoS_2 heterojunction can be deconvoluted into the C–C (284.5 eV), C–O (285.9 eV), C=O (287.3 eV) and O–C=O (288.7 eV) peaks (dashed lines) [27, 28]. Compared with graphene in figure 3(b), the C–C peak is weaker, but the C–O, C=O and O–C=O peak intensities are much higher in graphene/MoS_2 heterojunction, which are the defects in graphene for both samples treated by UV/O_3. This comparison shows that many more oxygen-containing groups and

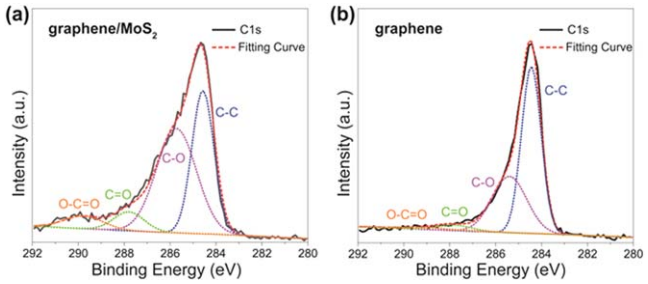

Figure 3. XPS spectra of C1s of (a) the graphene/MoS_2 heterojunction and (b) graphene with 4 min UV/O_3 treatment.

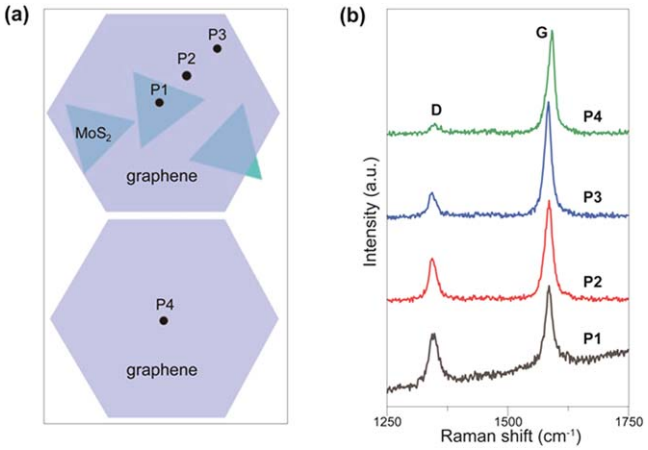

Figure 4. (a) Schematic diagram of the graphene/MoS_2 and graphene samples with the labeled positions on the surfaces of graphene/MoS_2 (P1), graphene near MoS_2 (P2), graphene far from MoS_2 (P3), pure graphene (P4). (b) Raman spectra tested at the four positions indicated in (a).

relatively broken C–C bonds in the graphene/MoS_2 heterojunction. In other words, more defects can be regarded as the higher oxidation degree of the UV/O_3 treated graphene. In addition, the XPS spectrum of C1s at 4 min is broadened relative to that at 0 min in figure S2 (supporting information). Then we test the Mo 3d spectrum and S 2p spectrum of MoS_2 as shown in figure S3 (supporting information). After the 4 min UV/O_3 treatment of the graphene/MoS_2 heterojunction, there are no peak for Mo–O bond at 236 eV [14, 29] and for S–O bond at about 165 eV [16] related to oxidation of MoS_2. It proves that MoS_2 is not oxidized, which might be due to the protection of the graphene overlayer against O_3 exposure, displaying the relatively intact structure of MoS_2 compared to graphene in the heterojunction.

After confirming that the existence of MoS_2 influences the oxidation degree of graphene in the heterojunction, we further investigate the effect of the distance between MoS_2 and graphene. For the typical graphene/MoS_2 sample with 4 min UV/O_3 exposure in figure 4(a), three positions with the distance between graphene and MoS_2 from near to far, which is on the surfaces of graphene/MoS_2 (P1), graphene near MoS_2 (P2), graphene far from MoS_2 (P3) are chosen for Raman measurements, with the position on the pure graphene (P4) taken as the infinity distance between graphene and MoS_2. The spot size of the excitation light used for Raman spectroscopy measurement is about one micron. With the help of a microscope, the four positions on the surfaces of the heterojunction and graphene can be accurately located. By comparing the intensity of the D peak at the four positions in Raman spectra of figure 4(b), it is clear that the D peak intensity is highest at the position with a shorter distance between graphene and MoS_2, indicating that graphene has a higher oxidation degree when MoS_2 gets closer to it. In addition, we test the Raman spectra of the heterojunction and graphene samples at the four positions without UV/O_3 treatment as comparison (see figure S4, supporting information). The results show all the D peaks of Raman spectra at four positions without UV/O_3 treatment are indiscernible, while the different D peak intensities at four positions appear after UV/O_3 treatment. This comparison indicates that the variation of the D peaks of Raman spectra of graphene at different positions in figure 4 mainly depends on the defects induced by UV/O_3 treatment. Therefore, we can confirm that MoS_2 can affect not only the graphene in the heterojunction, but also the graphene around the heterojunction when UV/O_3 is performed. And the influence of MoS_2 on graphene gradually weakens as their distance gets farther.

Then, in order to prove the electron concentration change of MoS_2 with the evolution of the graphene/MoS_2 heterojunction, we employ the micro-photoluminescence (PL) spectroscopy, with the approximate one micron spot size of the excitation light and the assistance of the microscope to ensure that the position of the heterojunction can be accurately located. Accurate test results can be obtained by controlling the laser power within the linear test range of the instrument. And we use the same laser wavelength (514 nm) and the same laser power for each measurement. There is no discernable peak of graphene in our PL spectrum measurement range (see figure S5, supporting information). Therefore, figure 5(a) displays the evolution of PL spectra of MoS_2 in heterojunction with different UV/O_3 expose time, and the corresponding changes of the position and intensity of the PL peak are plotted in figures 5(b) and (c), respectively. The PL peak intensity of MoS_2 in heterojunction with 1 min UV/O_3 treatment time reduces and the peak position shows a redshift compared to the untreated heterojunction. With increasing the exposure time from 1 to 5 min, the peak position gradually shows blueshift and the peak intensity basically keeps increasing. We have also added the error bar graphs of PL peak position and intensity of heterojunction, and the results show the same trend as figures 5(b) and (c) (see figure S6, supporting information). In addition, the PL peak comes from the competition between the negatively charged trion and the exciton of MoS_2 in heterojunction [16]. When PL spectra are dominated by trion recombination, lower energy emission leads to the redshift of the PL peak. On the contrary, it causes high intensity and blueshift of the PL peak. As shown in figures 5(b) and (c), the redshift and decrease in intensity of the PL peak indicate that the trion recombination increases and therefore the electrons increase of MoS_2 in the heterojunction with increasing the exposure time from 0 to 1 min. From 1 to 5 min, the PL peak blueshift and intensity

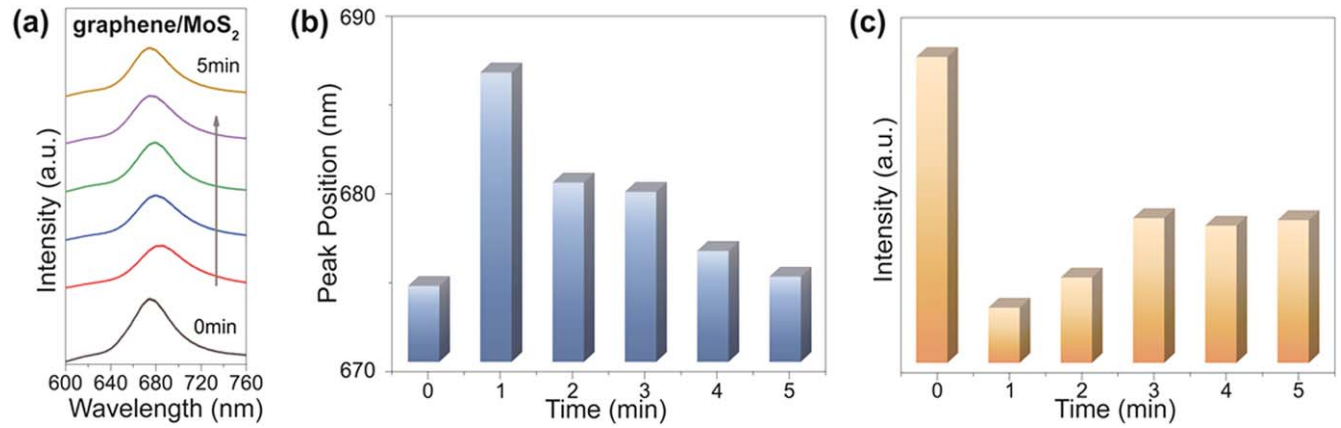

Figure 5. (a) PL spectra of graphene/MoS_2 without UV/O_3 treatment and with the UV/O_3 treatment for 1–5 min (b) Peak positions and (c) intensities of the graphene/MoS_2 heterojunction extracted from (a). The PL excitation wavelength is 514 nm.

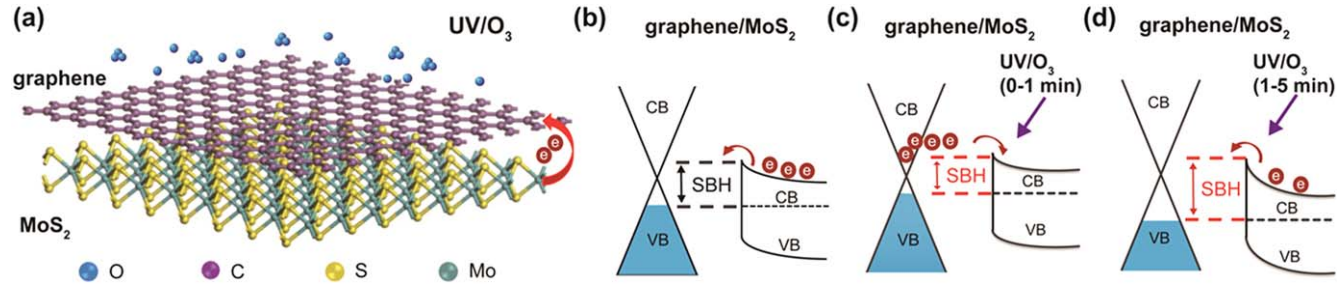

Figure 6. (a) Schematic diagram of interfacial charge transfer in graphene/MoS_2 with UV/O_3 treatment, purple balls represent carbon atoms, green and yellow balls represent Mo and S atoms in MoS_2, and blue balls represent oxygen atoms, respectively. (b) Band structure of graphene/MoS_2 heterojunction. Band structure of graphene/MoS_2 heterojunction with UV/O_3 treatment time (c) from 0 to 1 min and (d) from 1 to 5 min CB: conductance band, VB: valence band, SBH: Schottky barrier height.

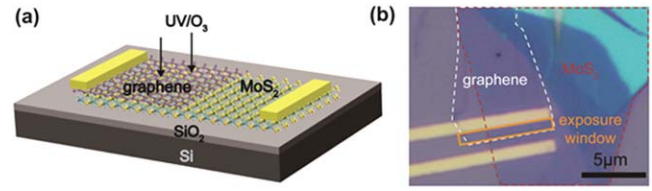

Figure 7. (a) A schematic diagram showing the FET device structure based on the graphene/MoS_2 heterojunction. (b) Optical image of the representative FET device.

enhancement indicate the decrease of trions recombination and therefore the electrons decrease of MoS_2 in the heterojunction. The evolution of the PL peak proves the change of electrons of MoS_2 in graphene/MoS_2 heterojunction during the UV/O_3.

Based on the above data, we analyze the underlying mechanism for the change of the structure and interfacial charge transfer property in the graphene/MoS_2 heterojunction with varying UV/O_3 exposure time as shown in figure 6. In general, graphene is p-doped due to many factors such as adsorbates and polymer residues, with a work function of 4.5 eV at the Dirac point, and MoS_2 is an n-type material due to its sulfur vacancies and other lattice impurities, and its Fermi level is close to the conductance band (CB) with an electron affinity energy of 4.0 eV and a bandgap of 1.8 eV [11, 30]. As graphene and MoS_2 contact to form the heterojunction, the band structure of MoS_2 deflects upward at the interface to form a Schottky barrier contact, and the difference in their work function triggers electron transfer from n-type MoS_2 to p-doped graphene in figure 6(b). During the 1 min treatment process, hole doping adsorbates, such as oxygen molecules, and polymer residues on the graphene [31] are removed by UV/O_3, keeping undamaged graphene structure and resulting in the upshift of the Fermi level and work function reduction of graphene in the heterojunction as shown in figure 6(c). This leads to the electron transfer from graphene to MoS_2 and the increase of the electron concentration in MoS_2, which induces trion recombination, as proved by the decrease of intensity and the redshift of position of the PL peak. With increasing treatment time from 1 to 5 min, the excited electrons from graphene are attracted to electronegative O_3 molecules absorbed on the graphene surface [13]. Then, the adsorbed O_3 molecules react with graphene to form more oxygen-containing groups, that is, more defect structures, which causes the p-doping of graphene [8]. This leads to the downshift of the Fermi level and the increase in work function of graphene in the heterojunction with increasing treatment time as shown in figure 6(d). At the same time, the decrease of the electron concentration in MoS_2 suppresses the trion recombination, corresponding to the increase of intensity and the blueshift of position of the PL peak from 1 to 5 min in figure 5. The electrons in MoS_2 can act as an electron source for graphene, allowing more

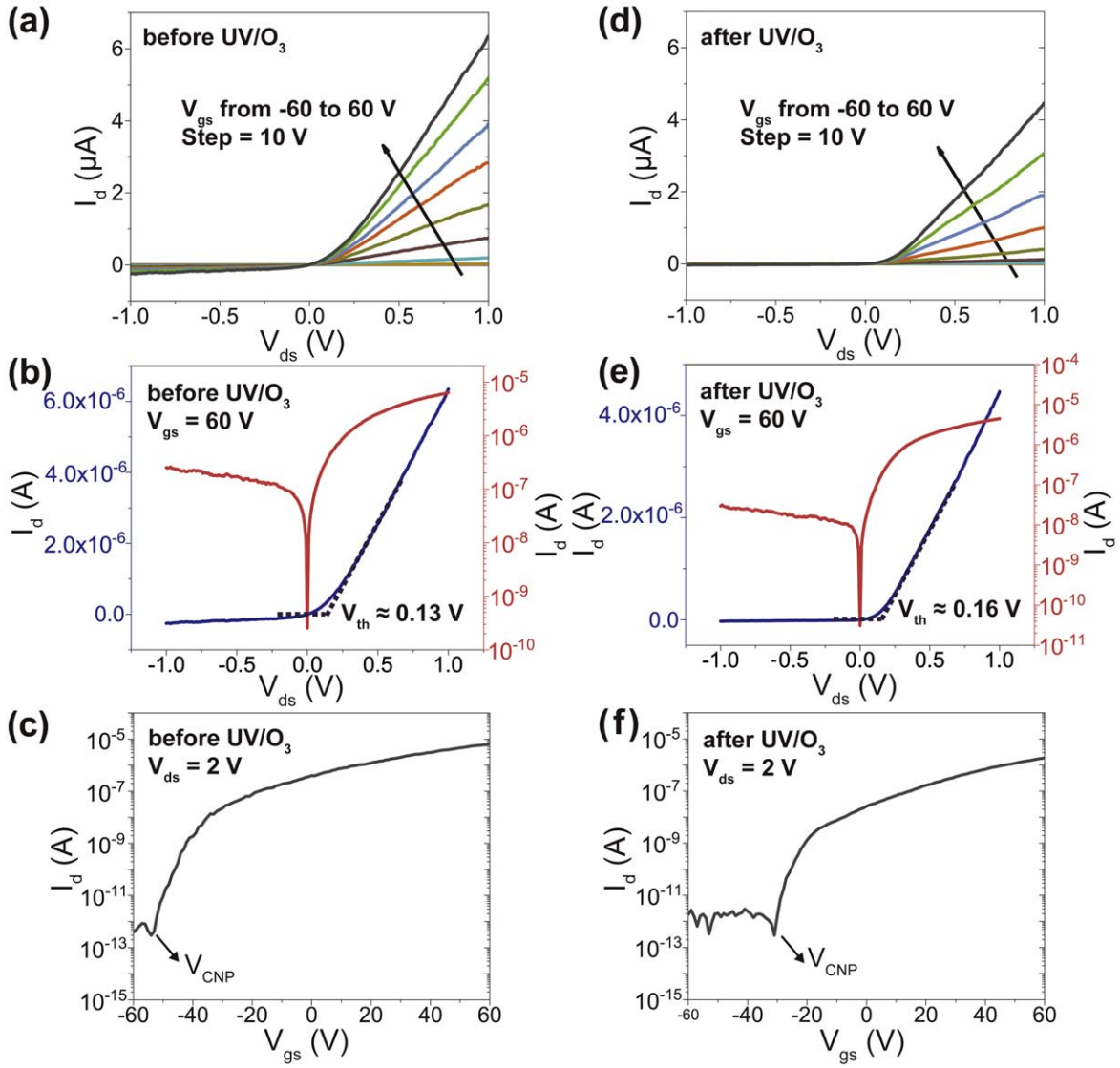

Figure 8. The experimental results of the graphene/MoS_2 heterojunction FET. (a) The output characteristics (I_d–V_{ds}) at various V_{gs} (the black arrow indicates the direction of increasing V_{gs}), (b) the output characteristics at $V_{gs} = 60$ V, the left axis represents a linear scale, and the right axis represents a log scale, (c) the transfer characteristics (I_d–V_{gs}) at $V_{ds} = 2$ V of the FET before UV/O_3 treating. (d)–(f) are the characteristics corresponding to (a)–(c) after UV/O_3 treating for 4 min V_{CNP}: the voltage of the charge neutrality point, corresponding to the position with minimum current. I_d: current. V_{ds}: bias voltage. V_{gs}: gate voltage.

electrons in graphene to react with O_3 molecules, promoting the adsorption of O_3 molecules and the generation of oxygen-containing groups.

The FET device is an important application of the graphene/MoS_2 heterojunction and we next study the effect of UV/O_3 on it. Mechanical exfoliated materials have higher quality than CVD heterojunctions. Moreover, it can reduce the polymer residue of wet transfer and the pattern etching process of CVD materials in the device manufacturing, and simplify the preparation process. Therefore, we adopt the mechanical exfoliated graphene and MoS_2 to study the electrical properties of the heterojunction. The mechanical exfoliated samples have similar Raman results with the samples synthesized by the CVD method (see figures S7 and S8, supporting information). The 4 min UV/O_3 treatment causes defects in the mechanical exfoliated heterojunction, thereby regulating the properties of the FET. Moreover, this defect degree will not seriously degrade the transistor performance. The schematic structure and representative optical image of the device as shown in figures 7(a) and (b). In figure 7(b), the white and red dashed boxes represent the positions of graphene and MoS_2, respectively. And the orange solid box is the position of graphene treated by UV/O_3. The contact between graphene and MoS_2 forms a Schottky junction, and the drain electrode is connected to MoS_2 to apply bias voltage, while the source electrode is grounded with graphene.

Here, we choose the graphene/MoS_2 heterojunction FET with 4 min UV/O_3 treatment as a representative device, and the FET without UV/O_3 treatment as a comparison. Figure 8 illustrates the electrical properties of the graphene/MoS_2 heterojunction FET. As shown in figures 8(a) and (d), the output characteristics curves at various V_{gs} show that the

conductivity and current increase with the increase of the gate voltage, which indicates the FET has gate tunable properties. In figures 8(b) and (e), the threshold voltage increases from 0.13 V before UV/O_3 to 0.16 V after UV/O_3. The change is negligible, and such low threshold voltages of FETs are promising for low-voltage operation. From these results, we can calculate that the rectification ratio at $|V_{ds}| = 0.5$ V is about 14 and 101 before and after UV/O_3 treatment respectively, improving by 7 times.

In figures 8(c) and (f), the transfer characteristics curves of the FET show that the on/off ratio can reach 10^6 at $V_{ds} = 2$ V indicating enormous application potential in the logic device community. We estimate the carrier mobility of FET before and after UV/O_3 by

$$\mu_{FE} = \frac{\partial I_d}{\partial V_{gs}} \frac{L}{WC_{ox}V_{ds}},$$

where L, W, C_{ox} and g_m are the channel length, width, gate capacitance per area, and the transconductance. When $V_{ds} = 2$ V, the carrier mobility before and after UV/O_3 are 163.34 $cm^2\,V^{-1}\,s^{-1}$ and 63.42 $cm^2\,V^{-1}\,s^{-1}$, respectively. The carrier mobility is reduced after UV/O_3, which is due to the generation of defects and the increase of Schottky barrier height. And it can be clearly seen from the transfer characteristics curves of FET that the V_{CNP} moves from −54 to −31 V after UV/O_3 at $V_{ds} = 2$ V. And the values of V_{CNP} at different bias voltages all shift to a positive gate voltage direction after UV/O_3 (see figure S9, supporting information). The change in V_{CNP} indicates that the p-doping of graphene in the heterojunction is enhanced after UV/O_3. The enhanced p-doping causes a downshift of the Fermi level of graphene, thereby increasing the Schottky barrier height of the graphene/MoS_2 heterojunction as illustrated in figure 6(d). The higher Schottky barrier height leads to an increase in the rectification ratio of FET. In addition, the output and transfer characteristics curves show that the currents have slightly decreased after UV/O_3. It might be caused by the generation of defects and the higher Schottky barrier height of the graphene/MoS_2 heterojunction.

4. Conclusion

In summary, we investigate the influence of UV/O_3 on the band structure of 2D graphene/MoS_2 van der Waals heterojunction. The structural changes of graphene can modulate the interfacial charge transfer, which can change the band structure of heterojunction. In addition, the corresponding change of electrical transport characteristics of graphene/MoS_2 heterojunction FET indicates the evolution of the Schottky barrier height and the band structure modulation of heterojunction by UV/O_3. Our work is beneficial to both fundamental research and practical applications of 2D van der Waals heterojunctions in the future.

Acknowledgments

The authors acknowledge financial support for this work from the National Key R&D Program of China (2018YFE0205400), the Strategic Priority Research Program of CAS (XDB36000000), the National Natural Science Foundation of China (21422303, 21573049, 21872043, 22002028), the National Basic Research Plan of China (2016YFA0201600), and the Beijing Natural Science Foundation (2142036).

Data availability statement

All data that support the findings of this study are included within the article (and any supplementary files).

ORCID iDs

Haitao Dai https://orcid.org/0000-0001-5424-6047
Jian Ru Gong https://orcid.org/0000-0003-1512-4762

References

[1] Novoselov K S, Mishchenko A, Carvalho A and Castro Neto A H 2016 2D materials and van der Waals heterostructures *Science* **353** aac9439
[2] Haque F, Daeneke T, Kalantar-zadeh K and Ou J Z 2018 Two-dimensional transition metal oxide and chalcogenide-based photocatalysts *Nano-Micro Lett.* **10** 38–64
[3] Zhou X, Hu X, Yu J, Liu S, Shu Z, Zhang Q, Li H, Ma Y, Xu H and Zhai T 2018 2D layered material-based van der Waals heterostructures for optoelectronics *Adv. Funct. Mater.* **28** 1706587
[4] Chao L, Peng Z, David and Zhang W 2017 Devices and applications of van der Waals heterostructures *J. Semicond.* **38** 031005
[5] Yu W J, Liu Y, Zhou H, Yin A, Li Z, Huang Y and Duan X 2013 Highly efficient gate-tunable photocurrent generation in vertical heterostructures of layered materials *Nat. Nanotechnol.* **8** 952–8
[6] Hu Z, Wu Z, Han C, He J, Ni Z and Chen W 2018 Two-dimensional transition metal dichalcogenides: interface and defect engineering *Chem. Soc. Rev.* **47** 3100–28
[7] Guo X, Zafar A, Nan H, Yu Y, Zhao W, Liang Z, Zhang X and Ni Z 2016 Manipulating fluorescence quenching efficiency of graphene by defect engineering *Appl. Phys. Express* **9** 555021
[8] Huh S, Park J, Kim Y S, Kim K S, Hong B H and Nam J M 2011 UV/ozone-oxidized large-scale graphene platform with large chemical enhancement in surface-enhanced Raman scattering *Acs Nano* **5** 9799–806
[9] Novoselov K S, Geim A K, Morozov S V, Jiang D, Zhang Y, Dubonos S V, Grigorieva I V and Firsov A A 2004 Electric field effect in atomically thin carbon films *Science* **306** 666–9
[10] Li H, Li X, Park J, Tao L, Kim K K, Lee Y H and Xu J 2019 Restoring the photovoltaic effect in graphene-based van der Waals heterojunctions towards self-powered high-detectivity photodetectors *Nano Energy* **57** 214–2211
[11] Pham T, Ramnani P, Villarreal C C, Lopez J, Das P, Lee I, Neupane M R, Rheem Y and Mulchandani A 2019 MoS_2graphene heterostructures as efficient organic compounds sensing 2D materials *Carbon* **142** 504–5121
[12] Freedy K M, Sales M G, Litwin P M, Krylyuk S, Mohapatra P, Ismach A, Davydov A V and McDonnell S J 2019 MoS_2 cleaning by acetone and UV-ozone: geological and synthetic material *Appl. Surf. Sci.* **478** 183–8

[13] Azcatl A *et al* 2014 MoS_2 functionalization for ultra-thin atomic layer deposited dielectrics *Appl. Phys. Lett.* **104** 111601
[14] Park S, Kim S Y, Choi Y, Kim M, Shin H, Kim J and Choi W 2016 Interface properties of atomic-layer-deposited Al_2O_3 thin films on ultraviolet/ozone-treated multilayer MoS_2 crystals *ACS Appl. Mater. Interfaces* **8** 11189–93
[15] Wei Chen C *et al* 2012 UV ozone treatment for improving contact resistance on graphene *J. Vac. Sci. Technol.* B **30** 606041
[16] Jung C, Yang H I and Choi W 2019 Effect of ultraviolet-ozone treatment on MoS_2 monolayers: comparison of chemical-vapor-deposited polycrystalline thin films and mechanically exfoliated single crystal flakes *Nanoscale Res. Lett.* **14** 278
[17] Kim C, Moon I, Lee D, Choi M S, Ahmed F, Nam S, Cho Y, Shin H, Park S and Yoo W J 2017 Fermi level pinning at electrical metal contacts of monolayer molybdenum dichalcogenides *Acs Nano* **11** 1588–96
[18] Malard L M, Pimenta M A, Dresselhaus G and Dresselhaus M S 2009 Raman spectroscopy in graphene *Phys. Rep.* **473** 51–87
[19] Liang L and Meunier V 2014 First-principles Raman spectra of MoS_2, WS_2 and their heterostructures *Nanoscale* **6** 5394–401
[20] Guo B, Liu Q, Chen E, Zhu H, Fang L and Gong J R 2010 Controllable N-doping of graphene *Nano Lett.* **10** 4975–80
[21] Ferrari A C *et al* 2006 Raman spectrum of graphene and graphene layers *Phys. Rev. Lett.* **97** 187401
[22] Yu Q, Lian J, Siriponglert S, Li H, Chen Y P and Pei S 2008 Graphene segregated on Ni surfaces and transferred to insulators *Appl. Phys. Lett.* **93** 113103
[23] Li H, Zhang Q, Yap C C R, Tay B K, Edwin T H T, Olivier A and Baillargeat D 2012 From bulk to monolayer MoS_2: evolution of Raman scattering *Adv. Funct. Mater.* **22** 1385–90
[24] Liu K *et al* 2012 Growth of large-area and highly crystalline MoS_2 thin layers on insulating substrates *Nano Lett.* **12** 1538–44
[25] Basko D M, Piscanec S and Ferrari A C 2009 Electron-electron interactions and doping dependence of the two-phonon Raman intensity in graphene *Phys. Rev.* B **80** 1654131
[26] Tang B, Guoxin H and Gao H 2010 Raman spectroscopic characterization of graphene *Appl. Spectrosc. Rev.* **45** 369–4071
[27] Leconte N, Moser J, Ordejon P, Tao H, Lherbier A, Bachtold A, Alsina F, Sotomayor T C, Charlier J C and Roche S 2010 Damaging graphene with ozone treatment: a chemically tunable metal-insulator transition *Acs Nano* **4** 4033–8
[28] Cheng Y C, Kaloni T P, Zhu Z Y and Schwingenschlögl U 2012 Oxidation of graphene in ozone under ultraviolet light *Appl. Phys. Lett.* **101** 731101
[29] Yang X, Fu W, Liu W, Hong J, Cai Y, Jin C, Xu M, Wang H, Yang D and Chen H 2014 Engineering crystalline structures of two-dimensional MoS_2 sheets for high-performance organic solar cells *J. Mater. Chem.* A **2** 7727–33
[30] Rathi S *et al* 2015 Tunable electrical and optical characteristics in monolayer graphene and few-layer MoS_2 heterostructure devices *Nano Lett.* **15** 5017–24
[31] Chen C W, Ren F, Chi G, Hung S, Huang Y P, Kim J, Kravchenko I I and Pearton S J 2012 UV ozone treatment for improving contact resistance on graphene *J. Vac. Sci. Technol.* B **30** 060604